ACS APPLIED MATERIALS & INTERFACES

Research Article

www.acsami.org

One-Pot Synthesis of CdS and Ni-Doped CdS Hollow Spheres with Enhanced Photocatalytic Activity and Durability

Man Luo, Yong Liu, Juncheng Hu,* Hang Liu, and Jinlin Li

Key Laboratory of Catalysis and Materials Science of the State Ethnic Affairs Commission & Ministry of Education, Hubei Province, South-Central University for Nationalities, Wuhan 430074, P. R. China

ABSTRACT: CdS and Ni-doped CdS hollow spheres were synthesized via a simple template-free one-pot method. The products were characterized by X-ray powder diffraction, scanning electron microscopy, transmission electron microscopy, high-resolution transmission electron microscopy, energy-dispersive spectroscopy analysis, X-ray photoelectron spectroscopy, and UV−vis absorption spectroscopy. The formation mechanism for the Ni-doped CdS hollow spheres was discussed. The prepared CdS and Ni-doped CdS hollow spheres showed the superior photocatalytic activity for the degradation of RhB under visible light (λ > 420 nm) irradiation, and 1.2 mol % Ni-doped CdS hollow spheres were found to be highly efficient for organic pollutants RhB and phenol removal. Moreover, this catalyst showed improved stability, and the activity did not decrease significantly after four recycles. The unique hollow spheres structure may favor the harvesting of exciting light due to multiple scattering within the interior space, and the doping of Ni^{2+} may facilitate the generation of electrons and holes pairs and inhibit their recombination rate by act as a temporary trapping sites of photoinduced electrons.

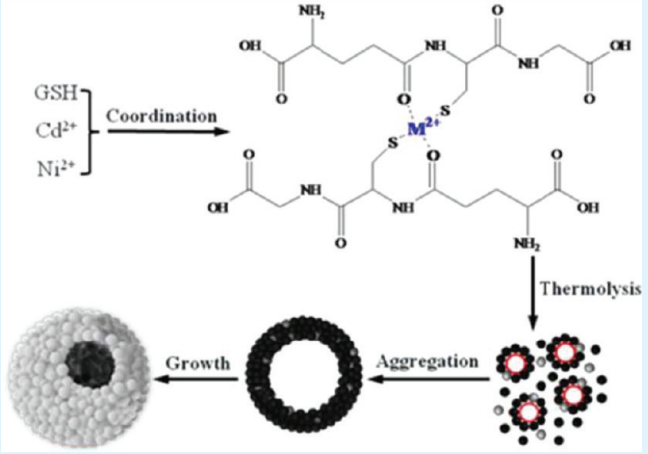

KEYWORDS: *hollow spheres, CdS, doping, nickel, photocatalysis*

1. INTRODUCTION

The crucial interplay among environmental pollution and energy utilization has garnered enormous research focus in these years. Semiconductor photocatalysts have a potential to utilize solar energy to solve many related problems, such as organic pollutants degradation and H_2 production from water splitting.[1−3] In recent years, virtually all the envisaged applications for photocatalysts require controllable synthesis of nanocrystal size and shape, thus allowing for improving their activity.[4−7] Because of the high light-harvesting efficiency, fast mobility of charge carriers, and superior catalytic activity,[8,9] hollow structured materials have been recognized as one type of promising material for applications in the field of photocatalytic processes.

CdS, a well-known visible-light-sensitive material,[10] has been widely studied for the conversion of solar energy into chemical energy. However, the low separation efficiency of photogenerated electrons and holes and the fact that it is easily corroded[11,12] are not favorable for the wide applications of CdS in environmental remediation and solar conversion. Therefore, it is highly desirable to develop highly efficient and robust visible-light responsive photocatalysts based on conventional semiconductor materials. Recent attempts to improve their photocatalytic performance focus on structure design or surface modification.[13−18] CdS with various nanostructures, such as nanowires, nanobelts, nanorods, and nanospheres have been prepared, while the achievement for increasing both the photoactivity and stability was not satisfying.[19−22] Considering that many metal ions doping (such as Mn, Co, Fe, Ni, etc.)[23−26] are demonstrated to control the bandgap and absorption properties, especially Ni^{2+} doping,[26,27] which is able to improve the photoactivity of photocatalysts, this is the origin of our research impetus. And currently, some constituent complex nanomaterials with well-defined structures have been extensively explored to realize the combination of respective properties of each component or achieve cooperatively enhanced performances.[28,29]

Therefore, the design and fabrication of CdS and Ni-doped CdS hollow structure is one feasible strategy in photocatalytic processes. The advantages of this conception are as follows: hollow structure enables both the outer and inner surfaces of the catalyst to contact with the reactants, and allow light-scattering of visible light within the interior cavity to promote the light-harvesting efficiency.[30,31] Further, the incorporation of Ni^{2+} into the CdS lattice can provide them with intriguing properties inherited from the synergetic effect and is expected

Received: January 17, 2012
Accepted: March 3, 2012
Published: March 4, 2012

to be possible because the radius of Ni^{2+} is smaller than that of Cd^{2+}.

Herein, we report a simple template-free one-pot method to prepare CdS and Ni-doped CdS hollow spheres using biomolecule glutathione (GSH) as sulfur source and bubble source. A large-scale of uniformed and well dispersed CdS and Ni-doped CdS hollow spheres were obtained without traditional tedious and intricate template removal procedures. This one-step route provides both the expected hollow structure and the Ni^{2+} doping. A possible formation mechanism for the Ni-doped CdS hollow spheres is discussed. In addition, we experimentally demonstrate the as-prepared Ni-doped CdS hollow spheres have an enhanced photocatalytic activity and improved durability for organic pollutants removal. The probable effect factors for the activity and stability are also discussed in detail.

2. EXPERIMENTAL SECTION

2.1. Materials and Sample Preparation. Cadmium nitrate tetrahydrate ($Cd(NO_3)_2{\cdot}4H_2O$), L-Glutathione reduced (GSH) and Coumarin were purchased from Aladdin, Nickel nitrate hexahydrate ($Ni(NO_3)_2.6H_2O$) was provided by Kermel Reagent. Methanol, phenol, and rhodamine-B (RhB) were provided by Sinopharm Chemical Reagent Co., Ltd. (Shanghai, China). All chemicals were analytical grade and used as received. Deionized and doubly distilled water was used in this work. In a typical preparation, 5.5 mmol of GSH was dissolved in a mixed solution of 205 mL of deionized water and 25 mL of methanol. Then, appropriate molar ratios of $Cd(NO_3)_2{\cdot}4H_2O$ and $Ni(NO_3)_2.6H_2O$ with the sum mole number of Cd^{2+} and Ni^{2+} being 5.5 mmol were added slowly to the mixture. The Ni-doping concentration was designed as 1.2, 3, and 5 mol % (denoted as X mol % Ni-doped CdS), which was the mole ratio of the theoretical yield. After being continuously stirred for 24 h, the clear solution was transferred into an autoclave with a quartz inline. The autoclave was purged with Nitrogen for 3 times, and then a pressure of 10 bar nitrogen was imposed into autoclave. The solution was heated to 200 °C and maintained for 24 h. Subsequently, the autoclave was cooled to room temperature naturally. The obtained samples were filtered, washed with acetone for several times, and then dried at 60 °C in an oven overnight and finally about 0.77 g (96% yield) product was obtained. The same procedures are applied to synthesize CdS hollow spheres and NiS sample, respectively.

2.2. Characterization. The crystalline structure of the catalysts was studied by power X-ray diffraction (XRD) (Bruker D8 Advance; Cu Kα = 1.5404 Å). The XRD patterns were recorded within 2θ range from 10° to 80° at a scanning rate of 0.05°/s. The morphologies and sizes of the samples were observed by a transmission electron micrograph (TEM) and high-resolution transmission electron microscopy (HRTEM) analyses using a Tecnai G20 (FEI Co., Holland) microscope operated at accelerating voltage of 200 kV. The samples were prepared by dispersing the powder in acetone and dropping a drop of very dilute suspension onto a carbon film-coated copper grid. Energy dispersive spectrum analysis (EDS) system was connected to the TEM. Scanning electron micrographs (SEM) were performed with a S4800 field-emission SEM (FESEM, Hitachi, Japan) at an accelerating voltage of 5 kV and linked with an Oxford Instruments X-ray analysis system. X-ray photoelectron spectroscopy (XPS) measurements were conducted on a VG Multilab 2000 (VG Inc.) photoelectron spectrometer using Al Kα radiation as the excitation source under vacuum at 2×10^{-6} Pa. All the binding energy (BE) values were calibrated by the C 1s peak at 284.6 eV of the surface adventitious carbon. UV−vis diffused reflectance spectra were obtained for the dry-pressed disk samples using a UV−vis spectrometer (UV-2450, Shimadzu, Japan). BaSO4 was used as a reflectance standard in UV−vis diffuse reflectance experiments.

2.3. Photocatalytic Activity Measurement. The photocatalytic activity of the samples was evaluated by the degradation of Rhodamine B (50 mL, 1×10^{-5} mol L^{-1}) and phenol (50 mL, 20 mg L^{-1}) under visible light irradiation, respectively. In each experiment, 50 mg of catalysts was suspended in RhB or phenol solution. The suspensions were magnetically stirred in the dark for 3 h to ensure the establishment of an adsorption/desorption equilibrium between the organics and the catalyst, then the suspensions was vertically irradiated using a 350 W Xe lamp illumination with restricted visible-light radiation by a 420 nm cutoff filter. At given irradiation time intervals, 5 mL solution was sampled, centrifuged, and then filtered through a Millipore filter (pore size 0.45 μm) to remove the catalyst particulates. All experiments are tested in the same condition.

The concentration of the organic dyes was analyzed by the UV−vis spectrometer measurement (UV-2450, Shimadzu). Phenol in the reaction solution was analyzed on a Dionex high performance liquid chromatography (HPLC) instrument equipped with a Ultimate 3000 HPLC pump, Ultimate 3000 Variable wavelength Detector, and a intersil ODS-3 120 C18 reverse column (4.6 mm × 250 mm, particle size 5 μm, 120 Å, Dionex Bonded Silica products). The mobile-phase was 60% methanol and 40% water with a flow rate of 1 mL min^{-1}. Total organic carbon (TOC) in the solution after RhB and phenol removal was measured by Analyzer Multi N/C 3100 (Analytic Jena, Germany).

2.4. Analysis of Hydroxyl Radicals (·OH). The production of ·OH on the surface of the photocatalyst was detected by a photoluminescence (PL) method using coumarin as a probe molecule. Coumarin can readily react with ·OH to produce highly fluorescent product, 7-hydroxycoumarin.[32] Experimental procedure was similar to the measurement of photocatalytic activity. Coumarin (50 mL, 5×10^{-4} M) and Ni-doped CdS photocatalyst (50 mg) were mixed under magnetic stirring for 3 h under dark conditions. Then, the suspensions was irradiated under visible light (λ > 420 nm, use a cutoff filter of 420 nm). At given irradiation time intervals, the reaction solution was sampled and then filtered through a Millipore filter (pore size 0.45 μm) to measure the PL intensity around 445 nm excited by the wavelength of 332 nm.

3. RESULTS AND DISCUSSION

The XRD patterns of CdS and Ni-doped CdS samples are shown in Figure 1. All of these diffraction patterns are similar

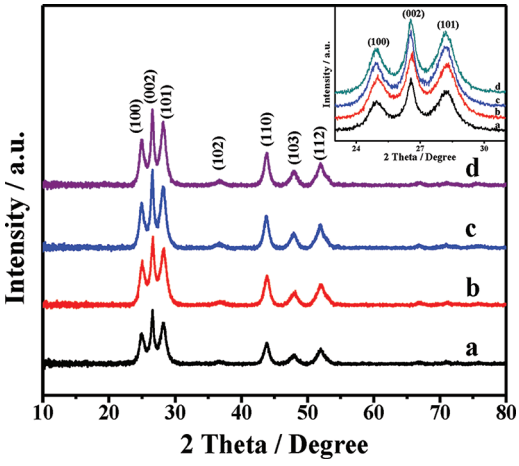

Figure 1. XRD patterns of Ni-doped CdS with different Ni doping concentrations (a) CdS, (b) 1.2 mol % Ni-doped CdS, (c) 3 mol % Ni-doped CdS, and (d) 5 mol % Ni-doped CdS. The inset is the enlarged (100), (002), and (101) peaks of Ni-doped CdS.

and can be assigned to hexagonal CdS according to JCPDS No.41−1049. Notably, the peak intensity of these samples increased slightly with the increase of Ni^{2+} doping concentration, suggesting these samples tend to be well crystallized. The average crystallite size was estimated based on the broadening of the (002) diffraction peak using the Scherrer

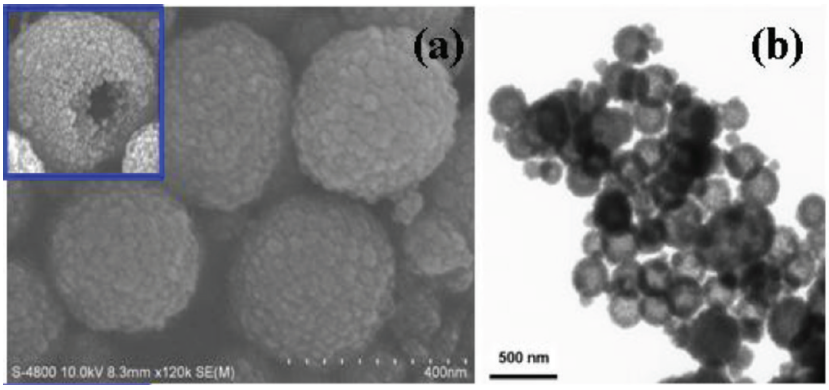

Figure 2. (a) SEM (the inset is an individual broken sphere) and (b) TEM image of CdS.

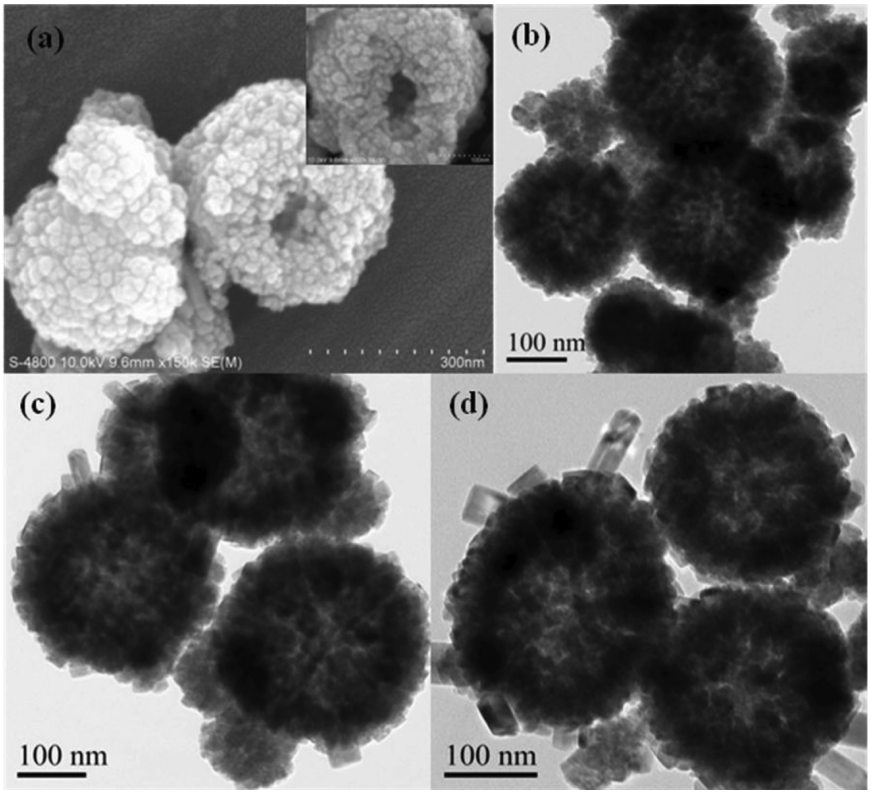

Figure 3. (a, b) SEM and TEM image of 1.2 mol % Ni-doped CdS, TEM images of (c) 3 mol % Ni-doped CdS and (d) 5 mol % Ni-doped CdS.

equation and is found to be 7.2, 10.2, 11.6, 12.7 nm for CdS, 1.2, 3, and 5 mol % Ni-doped CdS, respectively. The inset of Figure 1 reveals the enlarged (100), (002), and (101) diffraction peaks of these samples. It is observed that a slight shift toward higher 2θ values of 1.2 mol % Ni-doped CdS. The shift can partially contribute to the Ni^{2+} incorporated to CdS and occupied the substitutional cationic sites because the effective ionic radius of Ni^{2+} (6 coordinated radius: 0.69 Å) is smaller than that of Cd^{2+} (6 coordinated radius: 0.95 Å). It is noteworthy that there is no shift of these peaks for 3 and 5 mol % Ni-doped CdS. This observation may suggest that the portion of Ni^{2+} incorporated into the CdS lattice is not proportional to the doping concentration, that is, relatively low concentration of Ni^{2+} is easier to replace Cd^{2+}.

Figure 2 displays typical SEM and TEM images of pure CdS. All of the products are spherical-like structure with 200−300 nm diameters, and their external rough shells are composed of loosely packed nanoparticles (Figure 2a). From the broken sphere in the inset of Figure 2a, we can clearly find that the spheres have typical hollow interior structure. The TEM image of the corresponding sample CdS (Figure 2b) demonstrates the homogeneous morphology and good dispersity. The dark edge and pale center further confirms the hollow interior structure.

For Ni-doped CdS, SEM image in Figure 3a clearly reveals the hollow nature of these spheres and these spheres are composed of loosely packed nanoparticles, which make their surface rough. The images in Figure 3b−d are corresponding to the different Ni-doped CdS sample. We can find that the size of these spheres is about 200 nm in diameter and the shell thickness is about 80 nm. The edge of these spheres is darker than their center, indicating the hollow structures. There is no remarkable difference in the size and thickness of the spheres even the Ni^{2+} concentration increased to 5 mol %, but fewer nanorods are appeared in the edge of the spheres. These TEM images demonstrate the gradual change in morphology with the increase of Ni^{2+} concentration.

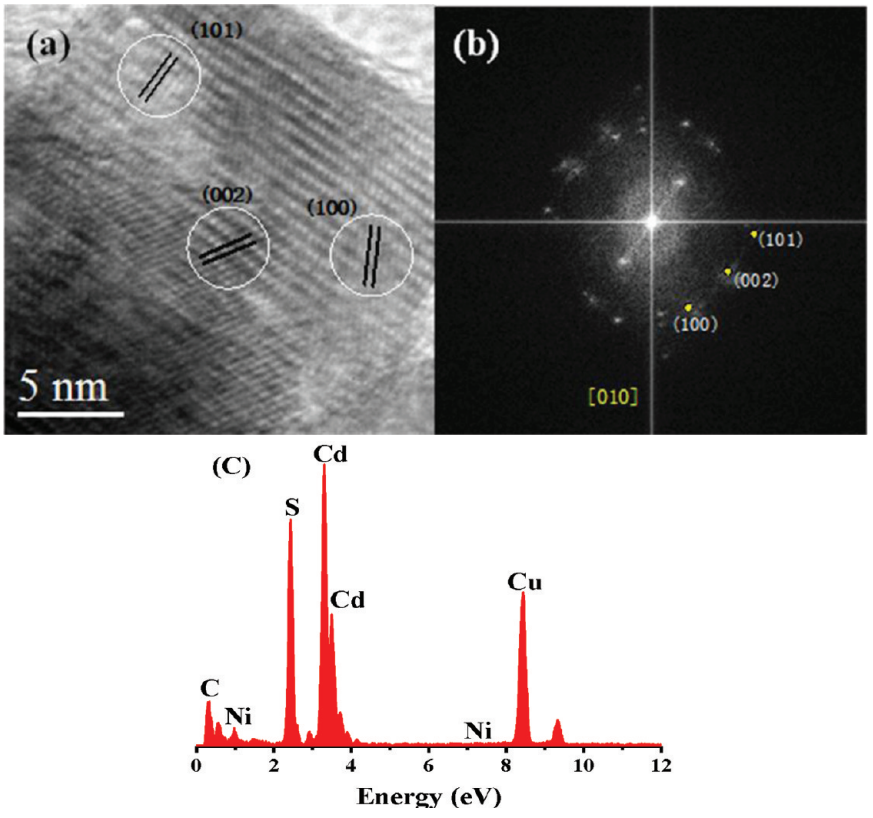

Figure 4. (a) HRTEM image, (b) FFT pattern, and (c) EDS image of 1.2 mol % Ni-doped CdS.

Scheme 1. Illustration of the Possible Formation Mechanism of Ni-Doped CdS Hollow Spheres

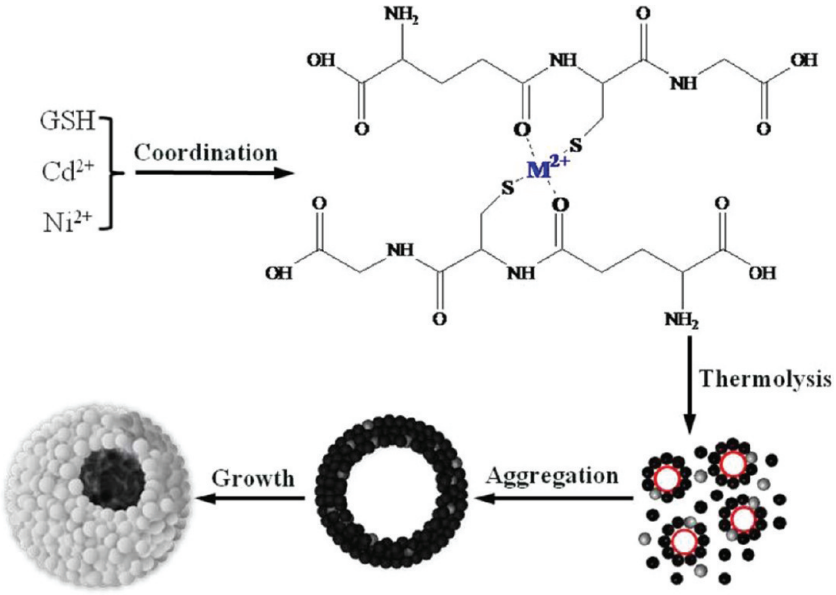

The high-resolution transmission electron microscopy (HRTEM) in Figure 4a exhibits three different lattice fringes, which correspond to the (100), (002), and (102) planes of hexagonal CdS, respectively. The corresponding fast Fourier transform (FFT) pattern is shown in Figure 4b. The energy-dispersive X-ray spectroscopy (EDS) analysis shown in Figure 4c confirms the presence of Cd, Ni, and S elements in the 1.2 mol % Ni-doped CdS sample.

Previous literature has reported that the biomolecule glutathione (GSH) had a strong tendency to coordinate with metal ions, and the presence of −SH, $-NH_2$, and −COOH groups could act as sulfur source and bubble source.[33,34] Scheme 1 illustrates the possible mechanism for the fabrication of Ni-doped CdS hollow spheres. First, Cd^{2+} and Ni^{2+} can coordinate with GSH, leading to the formation of metallic complex M^{2+}-GSH (M = Cd, Ni) as proposed in Scheme 1. Because of the relative stability of these complexes, the thermolysis proceeds slowly and leads to the formation of some Cd and Ni sulfide nuclei when heating the solution. These freshly formed nuclei in the solution are unstable and

contain a large number of dangling bonds, defects or traps on the nuclei surface,[35] which may contribute to the CdS crystalline formation and favor for the introducing of Ni^{2+} to the CdS crystalline. At higher temperature, because of the thermal and hydrolytic stability of the sulfur−metal bond, metal sulfide nanoparticles containing Ni−S−Cd are formed, together with the generation of CO_2 and NH_3 bubbles, which provide the assembly centers for the random moving metal sulfides nanoparticles. The attachment and the further aggregation of these nanoparticles on the gas/liquid interface form compact shells around the gas bubbles. The continuous aggregation process and the followed growth process are proposed to be responsible for the formation of Ni-doped CdS hollow spheres.

To investigate the surface information of the samples, pure CdS, and 1.2 and 5 mol % Ni-doped CdS samples were investigated by XPS. The signals of Ni 2p are very weak, and it is hard to be perceived due to the low doping concentration. Figure 5 provides the information of binding energies and intensities of the surface element of S 2p of CdS and 1.2 and 5 mol % Ni-doped CdS. The S 2p and Cd 3d peaks of CdS

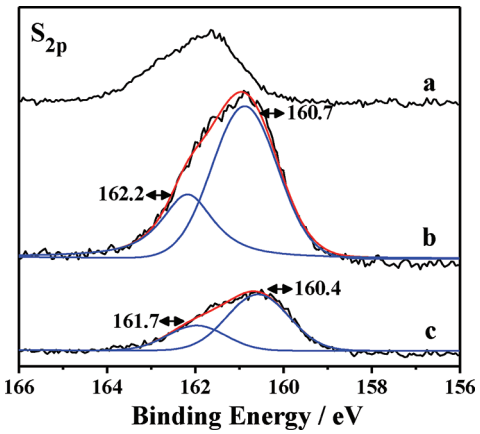

Figure 5. XPS results of S 2p of (a) CdS, (b) 1.2 mol %, and (c) 5 mol % Ni-doped CdS.

hollow spheres are at about 161.6 and 404.4 eV, which is in accordance with reference values (161.6 eV for S 2p and 404.5 eV for Cd 3d).[10,36] As the concentration of Ni^{2+} increases, the position of the peak shifts to a lower energy compared with pure CdS. This could be ascribed to some Cd^{2+} replaced by Ni^{2+} of the CdS lattice and the formation of Cd−S−Ni bonds in the Ni-doped CdS samples. The difference in electronegativity (χ) between Cd (χ_p = 1.69), S (χ_p = 2.56) and Ni (χ_p = 1.91) results in a higher electron cloud density of S atoms, thus the binding energy of S 2p (160.97 and 160.66 eV for 1.2% and 5% mol Ni-doped CdS respectively) decreases compared to pure CdS (161.6 eV). The asymmetric band of S 2p of Ni-doped CdS samples can be fitted into two peaks, the peaks at about 160.9 and 160.6 eV can be assigned to the S atoms bonded to the Cd atoms. Similarly, the peaks at about 162.2 and 162.0 eV can be assigned to the S atoms bonded to the Ni atoms which may arise from some Ni^{2+} replaced Cd^{2+} of the CdS lattice.

The UV−visible DRS spectra of CdS hollow spheres and Ni-doped CdS hollow spheres are shown in Figure 6. A strong absorption in the visible-light region can be assigned to the intrinsic bandgap absorption of CdS. After comparison, we find a red-shift for the Ni-doped CdS samples. This indicates that there is a decrease in energy band gap of these samples. The

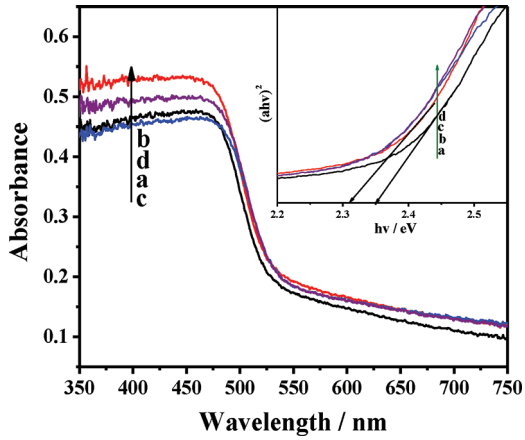

Figure 6. UV−vis DRS of (a) CdS, (b) 1.2 mol % Ni-doped CdS, (c) 3 mol % Ni-doped CdS, and (d) 5 mol % Ni-doped CdS . The inset is band gap evaluation from the plots of $(Ahv)^2$ versus photon energy (hv).

direct band gap values of the CdS and Ni-doped CdS samples were estimated from the $(\alpha h\nu)^2$ versus photon energy ($h\nu$) plot as shown in the insert of Figure 6. The band gaps of the Ni-doped CdS samples are approximately equal, and are estimated to be 2.31 eV, which is lower than that of CdS (2.35 eV). The above results show that the absorption spectrum is broadened and the band gap is narrowed by the doping of Ni^{2+}. Especially the 1.2 mol % Ni^{2+} doping concentration shows much higher intensity in the UV-light region and wider absorption edge in the visible-light region than that of the other samples, it indicates that this sample have greater carrier concentration, since the optical absorption in this wavelength region is due to free-carrier absorption of the conduction electrons. Thus it is speculated that this sample may have the highest visible-light-driven photocatalytic activity.

To demonstrate the potential applicability of Ni-doped CdS hollow spheres, the photocatalytic activities of these samples were compared by the degradation of dye RhB under visible-light irradiation (λ > 420 nm). The Degussa P25 was used as the reference. As shown in Figure 7, we can find that only a negligible activity is detected when the catalyst free or light off. In contrast, a remarkably high activity is observed in the

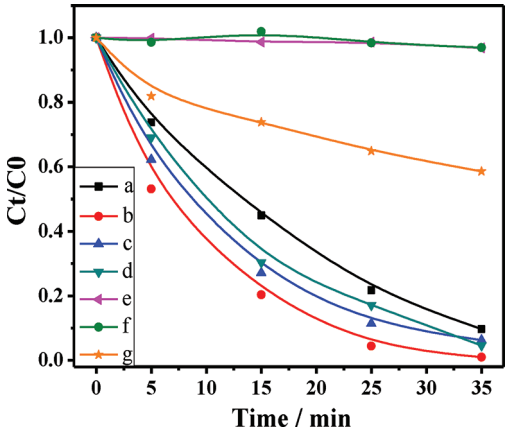

Figure 7. C_t/C_0 versus time curves of RhB photodegradation under visible-light (λ > 420 nm) irradiation over (a) CdS, (b) 1.2 mol % Ni-doped CdS, (c) 3 mol % Ni-doped CdS, (d) 5 mol % Ni-doped CdS, (e) catalyst free, (f) light off, and (g) Degussa P25.

presence of light and as-prepared undoped CdS hollow spheres or Ni-doped CdS hollow spheres compared with the Degussa P25. It is worthy noting that all the Ni-doped CdS samples show enhanced activities than that of undoped CdS hollow spheres, this result suggests that the insertion of Ni^{2+} can improve the photoactivity of CdS. While with the Ni^{2+} content increasing, the photoactivity of as-prepared samples is not be enhanced monotonously. The activity is not proportional to the Ni^{2+} doping concentration, this can be partly attributed to the differences in crystallite size and morphology. In addition, the relatively high doping concentrations of Ni^{2+} might cause a reduced adsorption of RhB and become the recombination center of photogenerated carriers, resulting in a decrease of photocatalytic efficiency.[25,37]

It is also found that the 1.2 mol % Ni−doped CdS hollow spheres shown the highest activity for the removal of RhB and RhB can be completely eliminated within 35 min. The superior activity is attributed to more efficient light harvesting by special structure and effective separation of photogenerated carries affected by optimal Ni^{2+} doping. Figure 8 shows the temporal evolution of the spectra of RhB over 1.2 mol % Ni-doped CdS hollow spheres under visible-light irradiation. It can be seen

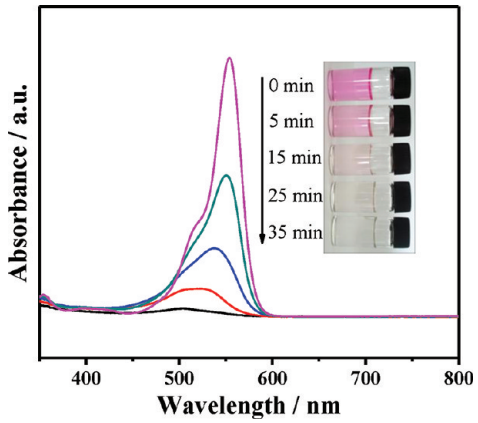

Figure 8. Temporal UV−vis absorption spectra of RhB (1.0×10^{-5} M, 50 mL) in the presence of 1.2 mol % Ni-CdS powder (50 mg) under visible-light (λ > 420 nm) irradiation.

that the concentration of RhB decreases quickly, and the absorption peak corresponding to RhB (λ = 554 nm) nearly disappears after 35 min.

The durability of 1.2 mol % Ni-doped CdS hollow spheres was tested by RhB degradation for four recycles. As shown in Figure 9, the catalyst can decompose RhB dye efficiently without significant deactivation after four times recycling. Figure 9 shows the degradation percentage maintained up to 98% even for the fourth cycle. The corresponding XRD patterns in Figure 10 have no notable differences before and after the photocatalytic recycles. It indicates that the Ni-doped CdS hollow spheres are photostable and not photocorroded in the degradation of RhB.

It is of importance to detect the main active species in the photocatalytic process for investigating the photocatalytic mechanism. Coumarin, a non- or weakly luminescent molecule, can produce strongly luminescent compounds 7-hydroxycoumarin for the detection of ·OH generated on the surface of the catalysts during the photocatalytic process.[38] Figure 11 shows the typical PL spectral changes observed during visible-light irradiation in the system of Ni-doped CdS hollow spheres and

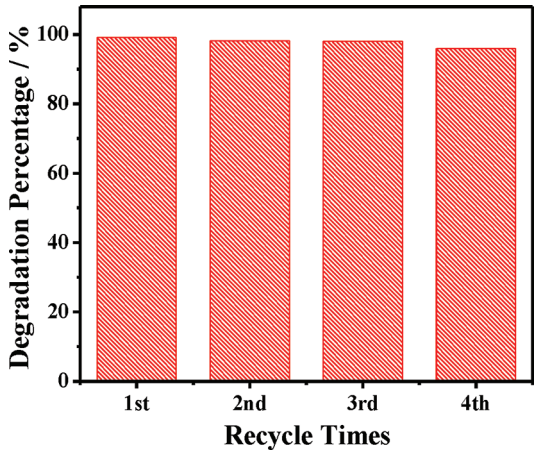

Figure 9. Degradation percentage of RhB in the presence of 1.2 mol % Ni-CdS powder (50 mg) under visible-light (λ > 420 nm) irradiation after 35 min.

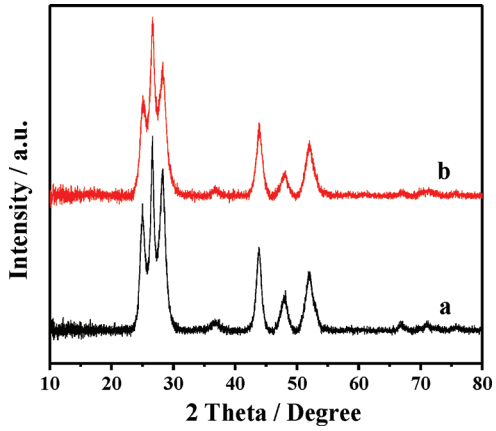

Figure 10. XRD patterns of (a) fresh 1.2 mol % Ni-doped CdS catalyst and (b) reused 1.2 mol % Ni-doped CdS catalyst after four times.

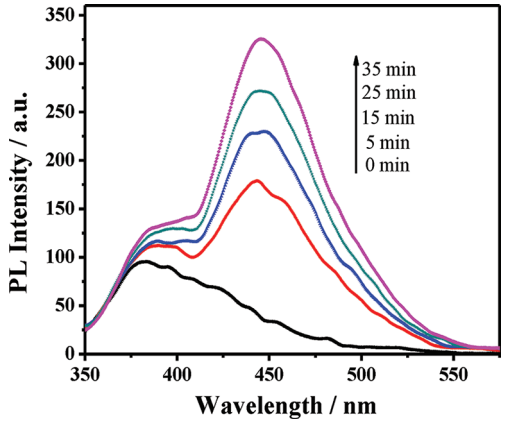

Figure 11. Time-dependent photoluminescence spectral changes in the presence of 1.2 mol % Ni-CdS hollow spheres and coumarin under visible-light (λ > 420 nm) irradiation.

coumarin. It is clearly seen that the PL intensity of photogenerated 7-hydroxycoumarin at about 450 nm (excited at 332 nm) increases with the irradiation time. This result indicates that the fast production of ·OH radicals and the highly accumulated ·OH radicals are the main active oxygen species in the photocatalytic process.

For the reactions of phenol with ·OH formed at the water/catalyst interface, it has been proposed that phenol is first oxidized to hydroquinone, *p*-benzoquinone, or muconaldehyde and then these products are converted into CO_2 via many oxidation steps.[39] The photocatalytic degradation of colorless pollutant phenol under visible light irradiation was also investigated by means of HPLC analysis of the intermediates. Figure 12 shows that the very symmetrical peak of phenol in the start of the reaction decreases gradually and nearly disappears after 4 h. Meanwhile, some new peaks appeared

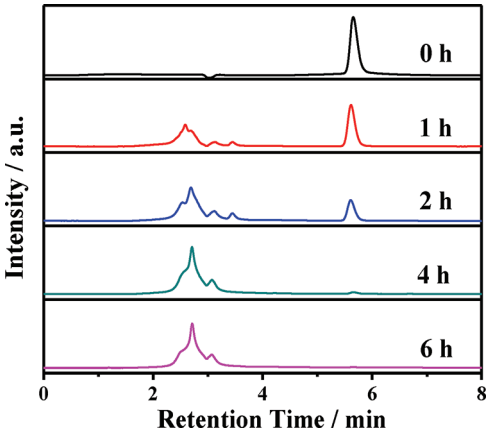

Figure 12. High-performance liquid chromatography (HPLC) analysis of phenol photodegradation over 1.2 mol % Ni-doped CdS hollow spheres under visible-light (λ > 420 nm) irradiation.

with the exposure time progresses, indicating intermediates or photodegradation products that similar to our recently reported work are formed.[40] It can be seen that the decomposition of organic pollutants phenol under visible light irradiation is rapid and efficient. Although these intermediates or photodegradation products seem to be fairly resistant to further oxidation and this can partly account for the fact that complete mineralization is not observed in this system.

For further investigating the photodegradation of RhB and phenol, we show the total organic carbon (TOC) removal during the degradation of RhB and phenol by 1.2 mol % Ni-doped CdS hollow spheres under visible-light irradiation in Figure 13. It can be seen that the TOC removal efficiency increases to 49.2% for RhB after 35 min and 63.3% for phenol after 360 min. These results further confirmed that RhB and phenol pollutants can be removed efficiently.

The Ni-doped CdS hollow spheres displayed an improved photoactivity in degradation of RhB. The higher activity may be ascribed to their unique structure as well as the Ni^{2+} doping. To validate that both of the attractive structure and the effective doping of Ni^{2+} contribute to the high activity, we compared the activities of the 1.2 mol % Ni-doped CdS hollow spheres with that of commercial CdS, physical mixture of NiS and CdS, undoped CdS hollow spheres, and NiS for the degradation of RhB under visible-light (λ > 420 nm) irradiation. The results presented in Figure 14 and the discussions are as follows: (1) undoped CdS hollow spheres and Ni-doped CdS hollow spheres show much higher photocatalytic activity than that of commercial bulk CdS, which could be ascribed to the unique hollow structure. The void interiors structure of Ni-doped CdS hollow spheres provides more active sites to interact with RhB molecules and allows multiple reflections of visible light within their interior cavities, which is very critical to achieve higher

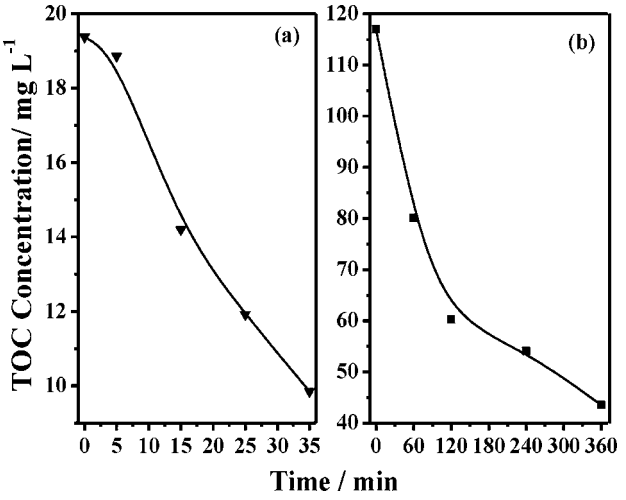

Figure 13. Total organic carbon (TOC) concentration of (a) RhB and (b) phenol photodegradation over 1.2 mol % Ni-doped CdS hollow spheres under visible-light (λ > 420 nm) irradiation.

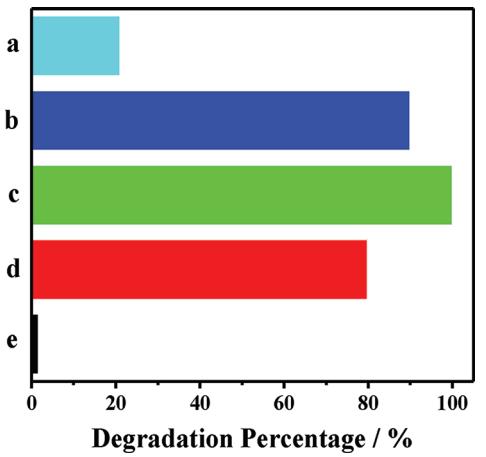

Figure 14. Activities of (a) commercial CdS, (b) undoped CdS hollow spheres, (c) 1.2 mol % Ni-doped CdS hollow spheres, (d) physical mixture of NiS and undoped CdS, and (e) NiS under visible-light (λ > 420 nm) irradiation.

light-harvesting efficiency, (2) pure NiS prepared in the same condition shows no obvious activity, and the mixture of pure NiS and CdS hollow spheres in the mole ratio of 1.2% displays a slightly lower activity than that of undoped CdS hollow spheres due to the decrease of active component. However, Ni-doped CdS hollow spheres show much higher activity than that of undoped CdS hollow spheres and the mixture of pure NiS and undoped CdS hollow spheres even though the doping concentration is very low. Noticeably, the enhanced photoactivity of the Ni-doped CdS hollow spheres implies that there may be some positive effect after Ni^{2+} doping.

On the basis of the above results, the probable mechanism of Ni^{2+} doping effect is also proposed as illustrated in Scheme 2. On the one hand, Ni^{2+} with partially filled d orbital creates an electron donor level in bandgap[41] when they partly entered the CdS lattice and thus narrowed the bandgap. The decreased band gap of Ni-doped CdS hollow spheres is more favorable to the harvesting of exciting light and the generation of electrons and holes pairs than undoped CdS hollow spheres under visible light irradiation. On the other hand, the doped Ni^{2+} can act as a temporary trapping site of photoinduced electrons and greatly

dx.doi.org/10.1021/am3000903 | ACS Appl. Mater. Interfaces 2012, 4, 1813−1821

Scheme 2. Diagram of the Proposed Photocatalytic Mechanism of Ni-Doped CdS under Visible-Light Irradiation

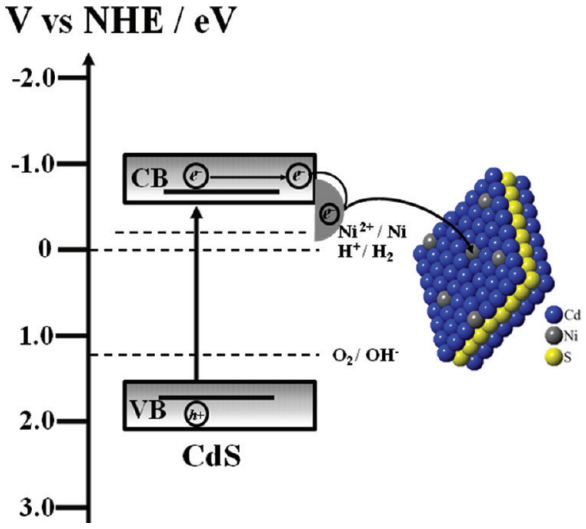

suppress the recombination of electron−hole pairs on the surface of the photocatalyst. This is similar to the case for Ni-doped TiO_2.[42] In addition, considering the coordination of Ni^{2+} and Cd^{2+} with the GSH ligands, it is speculated that NiS could be spontaneously formed when the hydrolysis of Ni^{2+}-GSH complexes. The potential of Ni^{2+}/Ni is about −0.23 V (vs SHE, pH 0), which is less negative than the CB level of CdS (about −0.7 V), the photoexcited electrons in the CB of CdS can transfer to NiS and then effectively separate the photoexcited electrons and holes. The role of NiS is similar to the $Ni(OH)_2$[43] and CuS[44] in the recently published reports, and some other electron transport materials, such as conducting polyaniline (PANI)[45] or graphite[46] also have been reported to reduce the recombination rate of electron−hole species in the semiconductors under light irradiation. The lower recombination rate of the photoexcited electrons and holes prolong the lifetime of photongenerated carrier and thus greatly improve the photocatalytic activity and durability in the removal of organic dyes and pollutants.

4. CONCLUSIONS

In summary, we have successfully synthesized CdS and Ni-doped CdS hollow spheres via a simple template-free one-pot method. The catalysts have superior photocatalytic activity in the degradation of RhB under visible light irradiation. The 1.2 mol % Ni-doped CdS hollow spheres show an excellent performance for the remove of organic pollutants. The high photocatalytic activity can be attributed to the hollow structure as well as the Ni^{2+} doping. The hollow structure may favors for the harvesting of exciting light and facilitates the transportation of reactants and products within the interior space. The doped Ni^{2+} plays a key role in narrowing the band gap and reducing the recombination rate of photon-generated carriers, thus promoted the activity and stability of the catalyst. We expect that the method and idea presented in this work will provide a new way for the construction of highly efficient photocatalysts not only for CdS, but also for other semiconductor materials.

AUTHOR INFORMATION

Corresponding Author

*Tel: +86 27 67841302. E-mail: junchenghuhu@hotmail.com.

Notes

The authors declare no competing financial interest.

ACKNOWLEDGMENTS

The Project was sponsored by the Scientific Research Foundation for the Returned Overseas Chinese Scholars, State Education Ministry and Ministry of Human Resources and Social Security. This work was also supported by National Natural Science Foundation of China (20803096, 21073238), the NSF of Hubei Province (Distinguished Young Investigator Grant 2010CDA082), National Basic Research Program of China (Grant No: 2011CB211704) and Key Laboratory of Green Catalysis of Sichuan Institute of High Education (LYJ1108).

REFERENCES

(1) Roy, P.; Berger, S.; Schmuki, P. *Angew. Chem., Int. Ed.* **2011**, *50*, 2904−2939.
(2) Liu, S. W.; Yu, J. G.; Jaroniec, M. *J. Am. Chem. Soc.* **2010**, *132*, 11914−11916.
(3) Li, X. H.; Zhang, J. S.; Chen, X. F.; Fischer, A.; Thomas, A.; Antonietti, M.; Wang, X. C. *Chem. Mater.* **2011**, *23*, 4344−4348.
(4) Chen, Y. B.; Wang, L. Z.; Lu, G. Q.; Yao, X. D.; Guo, L. J. *J. Mater. Chem.* **2011**, *21*, 5134−5141.
(5) Liu, G.; Yu, J. C.; Lu, G. Q.; Cheng, H. M. *Chem. Commun.* **2011**, *47*, 6763−6783.
(6) Zhou, T. F.; Hu, J. C.; Li, J. L. *Appl. Catal. B* **2011**, *110*, 221−230.
(7) Xiong, J. Y.; Cheng, G.; Lu, Z.; Tang, J. L.; Yu, X. L.; Chen, R. *CrystEngComm* **2011**, *13*, 2381−2390.
(8) Ibáñez, M.; Fan, J. D.; Li, W. H.; Cadavid, D.; Nafria, R.; Carrete, A.; Cabot, A. *Chem. Mater.* **2011**, *23*, 3095−3104.
(9) Liu, Z. Y.; Bai, H. W.; Sun, D. *Appl. Catal. B* **2011**, *104*, 234−238.
(10) Wang, D. J.; Li, D. S.; Li, G.; Fu, F.; Zhang, Z. P.; Wei, Q. T. *J. Phys. Chem. C* **2009**, *113*, 5984−5990.
(11) Zhang, J.; Liu, S. W.; Yu, J. G.; Jaroniec, M. *J. Mater. Chem.* **2011**, *21*, 14655−14662.
(12) Davis, A. P.; Huang, C. P. *Water. Res.* **1991**, *25*, 1273−1278.
(13) Chen, F.; Zhou, R. J.; Yang, L. G.; Liu, N.; Wang, M.; Chen, H. Z. *J. Phys. Chem. C* **2008**, *112*, 1001−1007.
(14) Zong, X.; Wu, G. P.; Yan, H. J.; Ma, G. J.; Shi, J. Y.; Wen, F. Y.; Wang, L.; Li, C. *J. Phys. Chem. C* **2010**, *114*, 1963−1968.
(15) Li, G. S.; Zhang, D. Q.; Yu, J. C. *Environ. Sci. Technol.* **2009**, *43*, 7079−7085.
(16) Gao, T.; Wang, T. H. *Chem. Commun.* **2004**, *22*, 2558−2559.
(17) Choi, J.; Ryu, S. Y.; Balcerski, W.; Lee, T. K.; Hoffmann, M. R. *J. Mater. Chem.* **2008**, *18*, 2371−2378.
(18) Lv, X. J.; Huang, F. Q.; Mou, X. L.; Wang, Y. M.; Xu, F. F. *Adv. Mater.* **2010**, *22*, 3719−3722.
(19) Xiong, S. L.; Zhang, X. G.; Qian, Y. T. *Cryst. Growth Des.* **2009**, *9*, 5259−5265.
(20) T. Shanmugapriya, T.; Vinayakan, R.; Thomas, K. G.; Ramamurthy, P. *CrystEngComm* **2011**, *13*, 2340−2345.
(21) Shemesh, Y.; Macdonald, J. E.; Menagen, G.; Banin, U. *Angew. Chem., Int. Ed.* **2011**, *50*, 1185−1189.
(22) Sun, S. Q.; Li, T. *Cryst. Growth Des.* **2007**, *7*, 2367−2371.
(23) Kim, D. S.; Cho, Y. J.; Park, J.; Yoon, J. B.; Jo, Y. H. *J. Phys. Chem. C* **2007**, *111*, 10861−10868.
(24) Chandramohan, S.; Kanjilal, A.; Sarangi, S. N.; Majumder, S.; Sathyamoorthy, R.; Hong, C. H.; Som, T. *Nanoscale* **2010**, *2*, 1155−1159.
(25) Li, J. X.; Xu, J. H.; Dai, W. L.; Li, H. X.; Fan, K. N. *Appl. Catal. B* **2009**, *85*, 162−170.

(26) Dong, L. H.; Liu, Y.; Zhuo, Y. J.; Ying Chu, Y. *Eur. J. Inorg. Chem.* **2010**, 2504−2513.
(27) Kudo, A.; Sekizawa, M. *Chem. Commun.* **2000**, *15*, 1371−1372.
(28) Deng, Y. H.; Cai, Y.; Sun, Z. K.; Liu, J.; Liu, C.; Wei, J.; Li, W.; Liu, C.; Wang, Y.; Zhao, D. Y. *J. Am. Chem. Soc.* **2010**, *132*, 8466−8473.
(29) Zhou, L.; Zhao, D. Y.; Lou, X. W. *Angew. Chem., Int. Ed.* **2011**, *50*, 1−4.
(30) Huo, Y. N.; Miao, M.; Zhang, Y.; Zhu, J.; Li, H. X. *Chem. Commun.* **2011**, *47*, 2089−2091.
(31) Lou, X. W.; Archer, L. A.; Yang, Z. C. *Adv. Mater.* **2008**, *20*, 3987−4019.
(32) Liu, Y.; Hu, J. C.; Zhou, T. F.; Che, R. C.; Li, J. L. *J. Mater. Chem.* **2011**, *21*, 16621−16627.
(33) Belcastro, M.; Marino, T.; Russo, N.; Toscano, M. *J. Inorg. Biochem.* **2009**, *103*, 50−57.
(34) Zhao, L.; Tao, F. Q.; Quan, Z.; Zhou, X. L.; Yuan, Y. H.; Hu, J. C. *Mater. Lett.* **2012**, *68*, 28−31.
(35) Zhong, J. S.; Xiang, W. D.; Liu, L. J.; Yang, X. Y.; Cai, W.; Zhang, J. F.; Liang, X. J. *J. Mater. Sci. Technol.* **2010**, *26*, 417−422.
(36) Zong, X.; Yan, H. J.; Wu, G. P.; Ma, G. J.; Wen, F. Y.; Wang, L.; Li, C. *J. Am. Chem. Soc.* **2008**, *130*, 7176−7177.
(37) Zhang, X. H.; Jing, D. W.; Guo, L. J. *Int. J. Hydrogen Energy* **2010**, *35*, 7051−7057.
(38) Wang, Z. Y.; Lv, K. L.; Wang, G. H.; Deng, K. J.; Tang, D. G. *Appl. Catal. B: Environ.* **2010**, *100*, 378−385.
(39) Park, H.; Choi, W. *Catal. Today* **2005**, *101*, 291−297.
(40) Liu, Y.; Hu, J. C.; Ngo, C.; Prikhodkob, S.; Kodambaka, S.; Li, J. L.; Richards, R. *Appl. Catal. B* **2011**, *106*, 212−219.
(41) Navarro, R. M.; Alvarez-Galván, M. C.; Mano, J. A. V.; Al-Zahrani, S. M.; Fierroa, J. L.G. *Energy Environ. Sci.* **2010**, *3*, 1865−1882.
(42) Begum, N. S.; Ahmed, H. M. F.; Gunashekar, K. R. *Bull. Mater. Sci.* **2008**, *31*, 747−751.
(43) Ran, J. R.; Yu, J. G.; Jaroniec, M. *Green Chem.* **2011**, *13*, 2708−2713.
(44) Zhang, J.; Yu, J. G.; Zhang, Y. M.; Li, Q.; Gong, J. R. *Nano Lett.* **2011**, *11*, 4774−4779.
(45) Zhang, H.; Zhu, Y. F. *J. Phys. Chem. C* **2010**, *114*, 5822−5826.
(46) Li, Q.; Guo, B. D.; Yu, J. G.; Ran, J. R.; Zhang, B. H.; Yan, H. J.; Gong, J. R. *J. Am. Chem. Soc.* **2011**, *133*, 10878−10884.